The effect of rotation on plane waves in generalized thermo-microstretch elastic solid with one relaxation time for a mode-I crack problem

Kh. Lotfy[a)b)†] and Mohamed I. A. Othman[a)]

[a)] *Department of Mathematics, Faculty of Science, Zagazig University, P.O. Box* 44519, *Zagazig, Egypt*

[b)] *Department of Mathematics, Faculty of Science, almithnab, Qassim University, P.O. Box* 6666, *Almithnab, Kingdom of Saudi Arabia*

(Received 8 February 2011)

The present paper is aimed at studying the effect of rotation on the general model of the equations of the generalized thermo-microstretch for a homogeneous isotropic elastic half-space solid, whose surface is subjected to a Mode-I crack problem. The problem is studied in the context of the generalized thermoelasticity Lord–Şhulman's (L–S) theory with one relaxation time, as well as with the classical dynamical coupled theory (CD). The normal mode analysis is used to obtain the exact expressions for the displacement components, the force stresses, the temperature, the couple stresses and the microstress distribution. The variations of the considered variables through the horizontal distance are illustrated graphically. Comparisons of the results are made between the two theories with and without the rotation and the microstretch constants.

Keywords: Lord–Şhulman's theory, thermoelasticity, microrotation, microstretch

PACS: 46.25.Hf **DOI:** 10.1088/1674-1056/20/7/074601

1. Introduction

The linear theory of elasticity is of paramount importance in the stress analysis of steel, which is the commonest engineering structural material. To a lesser extent, the linear elasticity describes the mechanical behaviour of the other common solid materials, e.g., concrete, wood and coal. However, the theory does not apply to the behaviour of many newly synthetic materials of the elastomer and polymer types, e.g., polymethyl–methacrylate (perspex), polyethylene and polyvinyl chloride. The linear theory of micropolar elasticity is adequate for representing the behaviour of such materials. For ultrasonic waves, i.e., for the case of elastic vibrations characterized by high frequencies and small wavelengths, the influence of the body microstructure becomes significant. This influence of microstructure results in the development of new type of waves, which are not in the classical theory of elasticity. Metals, polymers, composites, solids, rocks, concrete are typical media with microstructures. More generally, most natural and manmade materials including engineering, geological and biological media, possess microstructures. Agarwal[1,2] studied thermo-elastic and magneto- thermo-elastic plane waves propagating in an infinite non-rotating medium respectively. Some problems in thermo- elastic rotating media were studied by Schoenberg and Censor,[3] Puri,[4] Roy Choudhuri and Debnath,[5,6] and Othman.[7,8] Othman[9,10] studied the effect of rotation in a micropolar generalized thermoelastic and thermo-viscoelasticity half-space with different theories. The propagation of plane harmonic waves in a rotating elastic medium without a thermal field has been studied. It was shown there that the rotation causes the elastic medium to be dispersive and anisotropic. These problems are based on more realistic elastic model, since earth, moon and other planets all have angular velocity.

Eringen and Şuhubi[11] and Eringen[12] developed a linear theory of micropolar elasticity. Othman[13] studied the relaxation effects in thermal shock problems of generalized magneto-thermoelastic waves in elastic half space with three theories.

Eringen[14] introduced a theory for microstretch elastic solids. That theory is a generalization of the theory of micropolar elasticity[12,15] and a special case of the micromorphic theory. The material points of the microstretch elastic solids can stretch and con-

†Corresponding author. E-mail: khlotfy_1@yahoo.com

© 2011 Chinese Physical Society and IOP Publishing Ltd

tract independent of their transformations and rotations. The microstretch is used to characterize composite materials and various porous media.[16] The basic results in the theory of micro stretch elastic solids can be found in the literature.[17−20]

A theory for thermo-microstretch elastic solids was introduced by Eringen.[16] In the frame-work of the theory of thermo-microstretch solids, Eringen established a uniqueness theorem for the mixed initial-boundary value problem. The theory was illustrated through the solution of one dimensional waves and comparing that with lattice dynamical results. The asymptotic behaviour of the solutions and an existence result were presented by Bofill and Quintanilla.[21] A reciprocal theorem and a representation of Galerkin type were presented by De Cicco and Nappa.[22] De Cicco and Nappa[23] extended the linear theory of thermo-microstretch elastic solids to permit the transmission of heat as thermal waves with finite speed. The theory is based on the entropy production inequality proposed by Green and Laws.[24] In Ref. [23], the uniqueness of the solution of the mixed initial-boundary-value problem was also investigated. The basic results and an extensive review on the theory of thermo-microstretch elastic solids can be found in Eringen's book.[17]

The coupled theory of thermo-elasticity has been extended by including the thermal relaxation time in the constitutive equations by Lord and Shulman[25] and Green and Lindsay.[26] These theories eliminate the paradox of the infinite the velocity of the heat propagation and are termed the generalized theories of thermo-elasticity. Othman and Lotfy[27] studied two-dimensional problem of generalized magneto-thermo-elasticity under the effect of temperature dependent properties. Othman and Lotfy[28] studied transient disturbance in a half-space under generalized magneto-thermoelasticity with moving internal heat source. Othman and Lotfy[29] studied plane waves in a generalized thermo-microstretch elastic half-space by using a general model of the generalized thermo-microstretch in a homogeneous isotropic elastic half space. Othman *et al.*[30] studied the generalized thermo-microstretch elastic medium with temperature dependent properties using different theories. Othman and Lotfy[31] studied the effect of magnetic field and inclined load on micropolar thermoelastic medium possessing cubic symmetry with three theories. The normal mode analysis was used to obtain the exact expression for the temperature distribution, the thermal stresses and the displacement components.

In recent years, considerable efforts have been devoted to the study of the failure and the cracks in solids. This is due to the application of the latter generally in industry and particularly in the fabrication of electronic components. Most of the studies of the dynamical crack problem are done using the equations from coupled or even uncoupled theories of thermo-elasticity.[32−35] This is suitable for most situations, in which long time effects are sought. However, when short time behaviour is important, as in many practical situations, the full system of generalized thermoelastic equations must be used.[16]

The purpose of the present paper is to obtain the normal displacement, the temperature, the normal force stress and the tangential couple stress in a microstretch elastic solid under the effect of rotation. The problem of generalized thermo-microstretch in an infinite space weakened by a finite linear opening Mode-I crack is solved for the above variables. The distributions of the variables are represented graphically. A comparison of the temperature, the stresses and the displacements is carried out between the generalized thermo-elasticity Lord–Şhulman (L–S) and the coupled theories for the propagation of waves in semi-infinite microstretch elastic solids.

2. Formulation of the problem

Following Eringen,[17] Lord and Şhulman,[25] we obtain the constitutive and the field equations for a linear isotropic generalized thermo-microstretch elastic solid in the absence of body forces. We use a rectangular coordinate system (x, y, z) having origins on the surface $y = 0$ and z axis pointing vertically into the medium. The thermoelastic plate is rotating uniformly with an angular velocity $\boldsymbol{\Omega} = \Omega \boldsymbol{n}$, where n is a unit vector representing the direction of the axis of rotation (Fig. 1). The basic governing equations of the linear generalized thermo-elasticity with rotation in the absence of body forces and heat sources are

$$\begin{aligned}&(\lambda+\mu)\boldsymbol{\nabla}(\boldsymbol{\nabla}\cdot\boldsymbol{u})+(\mu+k)\boldsymbol{\nabla}^2\boldsymbol{u}\\&+k(\boldsymbol{\nabla}\times\boldsymbol{\varphi})+\lambda_0\boldsymbol{\nabla}\varphi^*-\hat{\gamma}\boldsymbol{\nabla}T\\&=\rho[\ddot{\boldsymbol{u}}+\boldsymbol{\Omega}\times(\boldsymbol{\Omega}\times\boldsymbol{u})+2\boldsymbol{\Omega}\times\dot{\boldsymbol{u}}],\end{aligned}\tag{1}$$

$$\begin{aligned}&(\alpha+\beta+\gamma)\boldsymbol{\nabla}(\boldsymbol{\nabla}\cdot\boldsymbol{\varphi})-\gamma\boldsymbol{\nabla}\times(\boldsymbol{\nabla}\times\boldsymbol{\varphi})\\&+k(\boldsymbol{\nabla}\times\boldsymbol{u})-2\mathrm{k}\boldsymbol{\varphi}=j\rho\frac{\partial^2\boldsymbol{\varphi}}{\partial t^2},\end{aligned}\tag{2}$$

$$\begin{aligned}&\alpha_0\boldsymbol{\nabla}^2\varphi^*-\frac{1}{3}\lambda_1\varphi^*-\frac{1}{3}\lambda_0(\boldsymbol{\nabla}\cdot\boldsymbol{u})\\&+\frac{1}{3}\hat{\gamma}_1T=\frac{3}{2}\rho j\frac{\partial^2\varphi^*}{\partial t^2},\end{aligned}\tag{3}$$

$$K\boldsymbol{\nabla}^2 T = \rho C_{\rm e}\left(n_1+\tau_0\frac{\partial}{\partial t}\right)\dot{T} + \hat{\gamma}T_0\left(n_1+n_0\tau_0\frac{\partial}{\partial t}\right)\dot{e}+\hat{\gamma}_1 T_0\frac{\partial\varphi^*}{\partial t}, \quad (4)$$

$$\sigma_{il} = (\lambda_0\varphi^*+\lambda u_{r,r})\delta_{il}+(\mu+k)u_{l,i} + \mu u_{i,l}-k\varepsilon_{ilr}\varphi_r-\hat{\gamma}T\delta_{il}, \quad (5)$$

$$m_{il} = \alpha\varphi_{r,r}\delta_{il}+\beta\varphi_{i,l}+\gamma\varphi_{l,i}, \quad (6)$$

$$\lambda_i = \alpha_0\phi_i^*, \quad (7)$$

$$e = \frac{\partial u}{\partial x}+\frac{\partial w}{\partial z}. \quad (8)$$

where T is the temperature above the reference temperature T_0 chosen, so that $|(T-T_0)/T_0|<1$, λ, μ are the counterparts of Lame parameters, the components of the displacement vector $\boldsymbol{u}$ are u_i, t is the time, τ_0 the relaxation time, σ_{ij} are the components of the stress tensor, e is the dilatation, e_{ij} are the components of the strain tensor, j is the micro inertia moment, k, α, β, γ are the micropolar constants, α_0, λ_0, λ_1 are the microstretch elastic constants, ϕ^* is the scalar microstretch, $\boldsymbol{\varphi}$ is the rotation vector, m_{ij} is the couple stress tensor, δ_{ij} is the Kronecker delta, ε_{ijr} is the alternate tensor, the mass density is ρ, the specific heat at constant strain is $C_{\rm e}$ and the thermal conductivity is $K(\geq 0)$.

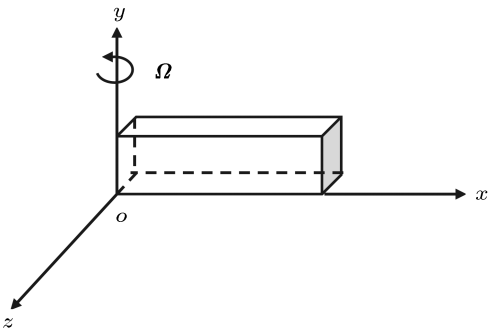


Fig. 1. Geometry of the problem.

The state of the plane strain parallel to the xz-plane is defined by

$$u_1=u(x,z,t),\quad u_2=0,$$
$$u_3=w(x,z,t),\quad \varphi_1=\varphi_3=0,$$
$$\varphi_2=\varphi_2(x,z,t),\quad \varphi^*=\varphi^*(x,z,t),\quad \boldsymbol{\Omega}=(0,\Omega,0). \quad (9)$$

The field Eqs. (1)–(4) reduce to

$$(\lambda+\mu)\left(\frac{\partial^2 u}{\partial x^2}+\frac{\partial^2 w}{\partial x\partial z}\right)+(\mu+k)\left(\frac{\partial^2 u}{\partial x^2}+\frac{\partial^2 u}{\partial z^2}\right)-k\frac{\partial\varphi_2}{\partial z}+\lambda_0\frac{\partial\varphi^*}{\partial x}-\gamma\frac{\partial T}{\partial x}=\rho\left(\frac{\partial^2 u}{\partial t^2}-\Omega^2 u+2\Omega\frac{\partial w}{\partial t}\right), \quad (10)$$

$$(\lambda+\mu)\left(\frac{\partial^2 u}{\partial x\partial z}+\frac{\partial^2 w}{\partial z^2}\right)+(\mu+k)\left(\frac{\partial^2 w}{\partial x^2}+\frac{\partial^2 w}{\partial z^2}\right)+k\frac{\partial\varphi_2}{\partial x}+\lambda_0\frac{\partial\varphi^*}{\partial z}-\hat{\gamma}\frac{\partial T}{\partial z}=\rho\left(\frac{\partial^2 w}{\partial t^2}-\Omega^2 w-2\Omega\frac{\partial u}{\partial t}\right), \quad (11)$$

$$\gamma\left(\frac{\partial^2\varphi_2}{\partial x^2}+\frac{\partial^2\varphi_2}{\partial z^2}\right)-2k\varphi_2+k\left(\frac{\partial u}{\partial z}-\frac{\partial w}{\partial x}\right)=j\rho\frac{\partial^2\varphi_2}{\partial t^2}, \quad (12)$$

$$\alpha_0\left(\frac{\partial^2\varphi^*}{\partial x^2}+\frac{\partial^2\varphi^*}{\partial z^2}\right)-\frac{1}{3}\lambda_1\varphi^*-\frac{1}{3}\lambda_0\left(\frac{\partial u}{\partial x}+\frac{\partial w}{\partial z}\right)+\frac{1}{3}\hat{\gamma}_1 T=\frac{3}{2}\rho j\frac{\partial^2\varphi^*}{\partial t^2}, \quad (13)$$

$$K\left(\frac{\partial^2 T}{\partial x^2}+\frac{\partial^2 T}{\partial z^2}\right)=\rho C_{\rm e}\left(n_1+\tau_0\frac{\partial}{\partial t}\right)\frac{\partial T}{\partial t}+\hat{\gamma}T_0\left(n_1+n_0\tau_0\frac{\partial}{\partial t}\right)\frac{\partial e}{\partial t}+\hat{\gamma}_1 T_0\frac{\partial\phi^*}{\partial t}, \quad (14)$$

where

$$\hat{\gamma}=(3\lambda+2\mu+k)\alpha_{t_1},\quad \hat{\gamma}_1=(3\lambda+2\mu+k)\alpha_{t_2},$$
$$\boldsymbol{\nabla}^2=\frac{\partial^2}{\partial x^2}+\frac{\partial^2}{\partial z^2}. \quad (15)$$

The constants $\hat{\gamma}$ and $\hat{\gamma}_1$ depend on the mechanical as well as the thermal properties of the body and the dot denotes the partial derivative with respect to time, α_{t_1}, $\alpha_{t_2}$are the coefficients of linear thermal expansions.

Equations (10)–(14) are the field equations of the generalized thermo-microstretch elastic solid. The L–S and the classical coupled theories can be obtained as follows:

(1) The equations of the coupled thermo-microstretch (CD) theory are obtained when

$$n_0=0,\quad n_1=1,\quad \tau_0=0. \quad (16)$$

Equations (10), (11), (13) and (14) have the form

$$\rho\left(\frac{\partial^2 u}{\partial t^2}-\Omega^2 u+2\Omega\frac{\partial w}{\partial t}\right) = (\lambda+\mu)\left(\frac{\partial^2 u}{\partial x^2}+\frac{\partial^2 w}{\partial x\partial z}\right)+(\mu+k)\left(\frac{\partial^2 u}{\partial x^2}+\frac{\partial^2 u}{\partial z^2}\right) - k\frac{\partial\varphi_2}{\partial z}+\lambda_0\frac{\partial\varphi^*}{\partial x}-\hat{\gamma}\frac{\partial T}{\partial x}, \quad (17)$$

$$\rho\left(\frac{\partial^2 w}{\partial t^2}-\Omega^2 w-2\Omega\frac{\partial u}{\partial t}\right)$$

$$= (\lambda+\mu)\left(\frac{\partial^2 u}{\partial x\partial z}+\frac{\partial^2 w}{\partial z^2}\right)+(\mu+k)\left(\frac{\partial^2 w}{\partial x^2}+\frac{\partial^2 w}{\partial z^2}\right) + k\frac{\partial\varphi_2}{\partial x}+\lambda_0\frac{\partial\varphi^*}{\partial z}-\hat{\gamma}\frac{\partial T}{\partial z}, \tag{18}$$

$$c_3^2\left(\frac{\partial^2\varphi^*}{\partial x^2}+\frac{\partial^2\varphi^*}{\partial z^2}\right)-c_4^2\varphi^* - c_5^2\left(\frac{\partial u}{\partial x}+\frac{\partial w}{\partial z}\right)+c_6^2 T=\frac{\partial^2\varphi^*}{\partial t^2}, \tag{19}$$

$$K\left(\frac{\partial^2 T}{\partial x^2}+\frac{\partial^2 T}{\partial z^2}\right) = \rho C_{\rm E}\frac{\partial T}{\partial t}+\hat{\gamma}T_0\frac{\partial e}{\partial t}+\hat{\gamma}_1 T_0\frac{\partial\varphi^*}{\partial t}. \tag{20}$$

The constitutive relation can be written as

$$\sigma_{xx}=\lambda_0\phi^*+(\lambda+2\mu+k)\frac{\partial u}{\partial x}+\lambda\frac{\partial w}{\partial z}-\hat{\gamma}T, \tag{21}$$

$$\sigma_{zz}=\lambda_0\phi^*+(\lambda+2\mu+k)\frac{\partial w}{\partial z}+\lambda\frac{\partial u}{\partial x}-\hat{\gamma}T, \tag{22}$$

$$\sigma_{xz}=\mu\frac{\partial u}{\partial z}+(\mu+k)\frac{\partial w}{\partial x}+k\varphi_2, \tag{23}$$

$$\sigma_{zx}=\mu\frac{\partial w}{\partial x}+(\mu+k)\frac{\partial u}{\partial z}+k\varphi_2, \tag{24}$$

$$m_{xy}=\gamma\frac{\partial\varphi_2}{\partial x}, \tag{25}$$

$$m_{zy}=\gamma\frac{\partial\varphi_2}{\partial z}, \tag{26}$$

where

$$c_3^2=\frac{2\alpha_0}{3\rho j},\quad c_4^2=\frac{2\lambda_1}{9\rho j},\quad c_5^2=\frac{2\lambda_0}{9\rho j},\quad c_6^2=\frac{2\hat{\gamma}_1}{9\rho j}. \tag{27}$$

(2) Lord–Şhulman (L–S) theory is obtained when

$$n_1=n_0=1,\quad \tau_0>0. \tag{28}$$

Equations (10), (11) and (13) are the same as Eqs. (17), (18) and (19) and Eq. (14) has the form

$$K\left(\frac{\partial^2 T}{\partial x^2}+\frac{\partial^2 T}{\partial z^2}\right) = \left(\frac{\partial}{\partial t}+\tau_0\frac{\partial^2}{\partial t^2}\right)(\rho C_{\rm e}T+\hat{\gamma}T_0 e) +\hat{\gamma}_1 T_0\frac{\partial\varphi^*}{\partial t}. \tag{29}$$

(3) The corresponding equations for the generalized micropolar thermoelasticity without the stretch can be obtained from the above mentioned cases by taking:

$$\alpha_0=\lambda_0=\lambda_1=\phi^*=0. \tag{30}$$

For convenience, the following dimensionless variables are used:

$$\bar{x}_i=\frac{\omega^*}{c_2}x_i,\quad \bar{u}_i=\frac{\rho c_2\omega^*}{\hat{\gamma}T_0}u_i,\quad \bar{t}=\omega^* t,$$

$$\bar{\tau}_0=\omega^*\tau_0,\quad \bar{\nu}_0=\omega^*\nu_0,\quad \bar{T}=\frac{T}{T_0},$$

$$\bar{\sigma}_{ij}=\frac{\sigma_{ij}}{\hat{\gamma}T_0},\quad \bar{m}_{ij}=\frac{\omega^*}{c_2\hat{\gamma}T_0}m_{ij},$$

$$\bar{\varphi}_2=\frac{\rho c_2^2}{\hat{\gamma}T_0}\varphi_2,\quad \bar{\lambda}_3=\frac{\omega^*}{c_2\hat{\gamma}T_0}\lambda_3,\quad \bar{\varphi}^*=\frac{\rho c_2^2}{\hat{\gamma}T_0}\varphi^*,$$

$$\omega^*=\frac{\rho C_{\rm e}c_2^2}{K},\quad \bar{\Omega}=\frac{\Omega}{\omega^*},\quad c_2^2=\frac{\mu}{\rho}. \tag{31}$$

Using Eq. (31), Eqs. (10)–(14) become (dropping the dashed for convenience)

$$\frac{\partial^2 u}{\partial t^2}-\Omega^2 u+2\Omega\frac{\partial w}{\partial t} = \frac{(\mu+k)}{\rho c_2^2}\boldsymbol{\nabla}^2 u+\frac{(\mu+\lambda)}{\rho c_2^2}\frac{\partial e}{\partial x}-\frac{k}{\rho c_2^2}\frac{\partial\varphi_2}{\partial z} +\frac{\lambda_0}{\rho c_2^2}\frac{\partial\varphi^*}{\partial x}-\frac{\partial T}{\partial x}, \tag{32}$$

$$\frac{\partial^2 w}{\partial t^2}-\Omega^2 w-2\Omega\frac{\partial u}{\partial t} = \frac{(\mu+k)}{\rho c_2^2}\boldsymbol{\nabla}^2 w+\frac{(\mu+\lambda)}{\rho c_2^2}\frac{\partial e}{\partial z}+\frac{k}{\rho c_2^2}\frac{\partial\varphi_2}{\partial x} +\frac{\lambda_0}{\rho c_2^2}\frac{\partial\varphi^*}{\partial z}-\frac{\partial T}{\partial z}, \tag{33}$$

$$\frac{j\rho c_2^2}{\gamma}\frac{\partial^2\varphi_2}{\partial t^2}=\boldsymbol{\nabla}^2\varphi_2-\frac{2kc_2^2}{\gamma\omega^*}\varphi_2+\frac{kc_2^2}{\gamma\omega^{*2}}\left(\frac{\partial u}{\partial z}-\frac{\partial w}{\partial x}\right), \tag{34}$$

$$\left(\frac{c_3^2}{c_2^2}\boldsymbol{\nabla}^2-\frac{c_4^2}{\omega^{*2}}-\frac{\partial^2}{\partial t^2}\right)\varphi^*-\frac{c_5^2}{\omega^{*2}}e+a_9 T=0, \tag{35}$$

$$\boldsymbol{\nabla}^2 T-(n_1+\tau_0\frac{\partial}{\partial t})\frac{\partial T}{\partial t} -\frac{\hat{\gamma}^2 T_0}{\rho K\omega^*}(n_1+n_0\tau_0\frac{\partial}{\partial t})\frac{\partial e}{\partial t}=\frac{\hat{\gamma}\hat{\gamma}_1 T_0}{\rho K\omega^*}\frac{\partial\varphi^*}{\partial t}. \tag{36}$$

Assuming the scalar potential functions $\varphi(x,z,t)$ and $\psi(x,z,t)$ defined by the relations in the dimensionless form:

$$u=\frac{\partial\varphi}{\partial x}+\frac{\partial\psi}{\partial z},\quad w=\frac{\partial\varphi}{\partial z}-\frac{\partial\psi}{\partial x}. \tag{37}$$

$$e=\boldsymbol{\nabla}^2\varphi. \tag{38}$$

Using Eq. (37) in Eqs. (32)–(36), we obtain

$$\left[\boldsymbol{\nabla}^2-a_0\frac{\partial^2}{\partial t^2}+a_0\Omega^2\right]\varphi-a_0 T +a_1\varphi^*+2\Omega a_0\frac{\partial\psi}{\partial t}=0, \tag{39}$$

$$\left[\boldsymbol{\nabla}^2-a_2\frac{\partial^2}{\partial t^2}+a_2\Omega^2\right]\psi-a_3\varphi_2-2\Omega a_2\frac{\partial\varphi}{\partial t}=0, \tag{40}$$

$$\left[\boldsymbol{\nabla}^2-2a_4-a_5\frac{\partial^2}{\partial t^2}\right]\varphi_2-a_4\boldsymbol{\nabla}^2\psi=0, \tag{41}$$

$$\left[a_6\boldsymbol{\nabla}^2-a_7-\frac{\partial^2}{\partial t^2}\right]\varphi^*-a_8\boldsymbol{\nabla}^2\varphi+a_9 T=0, \tag{42}$$

$$\left[\boldsymbol{\nabla}^2-(n_1\frac{\partial}{\partial t}+\tau_0\frac{\partial^2}{\partial t^2})\right]T$$
$$-\varepsilon\left(n_1\frac{\partial}{\partial t}+n_0\tau_0\frac{\partial^2}{\partial t^2}\right)\boldsymbol{\nabla}^2\varphi-\varepsilon_1\frac{\partial\varphi^*}{\partial t}=0, \quad (43)$$

where

$$c_1^2=\frac{\lambda+2\mu+k}{\rho}\quad a_0=\frac{c_2^2}{c_1^2},$$
$$a_1=\frac{\lambda_0}{\lambda+2\mu+k},\quad a_2=\frac{\rho c_2^2}{\mu+k},\quad a_3=\frac{k}{\mu+k},$$
$$a_4=\frac{kc_2^2}{\gamma}\omega^{*2},\quad a_5=\frac{\rho j c_2^2}{\gamma},\quad a_6=\frac{c_3^2}{c_2^2},$$
$$a_7=\frac{c_4^{2\,*2}}{\omega},\quad a_8=\frac{c_5^{2\,*2}}{\omega},\quad a_9=\frac{2\hat{\gamma}_1c_2^2}{9}\hat{\gamma}j\omega^{*2},$$
$$\varepsilon=\frac{\hat{\gamma}^2T_0}{\rho\omega^*K},\quad \varepsilon_1=\frac{\hat{\gamma}\hat{\gamma}_1T_0}{\rho\omega^*K}. \quad (44)$$

3. Normal mode analysis

The solution of the considering physical variables can be decomposed in terms of normal mode and are given in the following form:

$$[\phi,\psi,\,\varphi^*,\varphi_2,\sigma_{il},m_{il},T](x,z,t)$$
$$=[\bar{\varphi}(x),\bar{\psi}(x),\bar{\varphi}^*(x),\bar{\varphi}_2(x),\bar{\sigma}_{il}(x),\bar{m}_{il}(x),\bar{T}(x)]$$
$$\times\exp(\omega t+iaz). \quad (45)$$

where $[\bar{\phi},\bar{\psi},\,\bar{\phi}^*,\bar{\phi}_2,\bar{\sigma}_{il},\bar{m}_{il},\bar{T}](x)$ are the amplitudes of the functions, ω is a complex constant and a is the wave number in the z direction.

Using Eq. (45), then Eqs. (39)–(43) become

$$(\mathrm{D}^2-A_1)\bar{\varphi}-a_0\bar{T}+a_1\bar{\varphi}^*+A_2\bar{\psi}=0, \quad (46)$$
$$(\mathrm{D}^2-A_3)\bar{\psi}-a_3\bar{\varphi}_2-A_2\bar{\varphi}=0, \quad (47)$$
$$(\mathrm{D}^2-A_4)\bar{\varphi}_2-a_4(\mathrm{D}^2-a^2)\bar{\psi}=0, \quad (48)$$
$$(a_6\mathrm{D}^2-A_5)\bar{\varphi}^*-a_8(\mathrm{D}^2-a^2)\bar{\varphi}+a_9\bar{T}=0, \quad (49)$$
$$[(\mathrm{D}^2-a^2)-A_6]\bar{T}-A_7(\mathrm{D}^2-a^2)\bar{\varphi}-\varepsilon_1\omega\bar{\varphi}^*=0, \quad (50)$$

respectively, where $\mathrm{D}=\partial/\partial x$,

$$A_1=a^2+a_0(\omega^2-\Omega^2), \quad (51)$$
$$A_2=2\Omega a_0\omega,\quad A_2^*=2\Omega a_2\omega, \quad (52)$$
$$A_3=a^2+a_2(\omega^2-\Omega^2), \quad (53)$$
$$A_4=a^2+2a_4+a_5\omega^2, \quad (54)$$
$$A_5=a^2a_6+a_7+\omega^2, \quad (55)$$
$$A_6=\omega\,(n_1+\tau_0\omega)\,, \quad (56)$$
$$A_7=\varepsilon\omega\,(n_1+n_0\tau_0\omega)\,. \quad (57)$$

Eliminating $\bar{\varphi}_2$, $\bar{\psi}$, $\bar{\varphi}$, $\bar{T}$, and $\bar{\varphi}^*$ in Eqs. (46) and (50), we obtain the following tenth order ordinary differential equation for $\bar{\varphi}_2$, $\bar{\psi}$, $\bar{\varphi}$, $\bar{T}$, and $\bar{\varphi}^*$,

$$(\mathrm{D}^{10}-A\mathrm{D}^8+B\mathrm{D}^6-C\mathrm{D}^4+E\mathrm{D}^2-F)$$
$$\times\{\bar{\varphi}_2(x),\bar{\psi}(x),\bar{\varphi}(x),\bar{T}(x),\bar{\varphi}^*(x)\}=0. \quad (58)$$

Equation (58) can be factorized as

$$(\mathrm{D}^2-k_1^2)(\mathrm{D}^2-k_2^2)(\mathrm{D}^2-k_3^2)(\mathrm{D}^2-k_4^2)(\mathrm{D}^2-k_5^2)$$
$$\times\{\bar{\varphi}_2(x),\bar{\psi}(x),\bar{\varphi}(x),\bar{T}(x),\bar{\varphi}^*(x)\}=0. \quad (59)$$

where

$$A=(\,g_3+a_6g_1+a_6A_1+a_0a_6A_7-a_1a_8)/a_6, \quad (60)$$
$$B=[\,g_4+g_1(g_3+a_6A_1+a_0a_6A_7-a_1a_8)+a_6g_2$$
$$+A_1g_3+a_0g_7-a_1g_5+a_6A_2A_2^*]/a_6, \quad (61)$$
$$C=[\,g_1(g_4+a_0g_7-a_1g_5)+g_2(g_3-a_1a_8)$$
$$+A_1(g_4+g_1g_3+a_6g_2)+AA_2^*(g_3+a_6A_4)$$
$$+a_0(g_8+a_6A_2A_7)-a_1g_7]/a_6, \quad (62)$$
$$E=[\,g_2g_4+A_1(g_1g_4+g_2g_3)+a_0(g_1g_8+g_2g_7)-a_1$$
$$\times(g_1g_7+g_2g_5)+A_2A_2^*(g_4+A_4g_3)]/a_6, \quad (63)$$
$$F=[\,g_2(A_1g_4+a_0g_8-a_1g_7)+A_2A_2^*A_4g_4]/a_6. \quad (64)$$

with

$$g_1=A_3+A_4+a_3a_4,\quad g_2=A_3A_4+a^2a_3a_4,$$
$$g_3=A_5+a_6A_6^*,\quad g_4=A_5A_6^*-\varepsilon_1\omega a_9,$$
$$A_6^*=a^2+A_6,\quad g_5=a_8(A_6^*+a^2)-a_9A_7,$$
$$g_6=a^2(a_8A_6^*+a_9A_7),$$
$$g_7=A_7(A_5-a^2a_6)+\varepsilon_1\omega a_8,$$
$$g_8=a^2(A_5A_7-\varepsilon_1\omega a_8). \quad (65)$$

The solution of Eq. (58) has the form

$$\bar{\varphi}=\sum_{n=1}^{5}M_n(a,\omega)\,\mathrm{e}^{-k_nx}, \quad (66)$$
$$\bar{\psi}=\sum_{n=1}^{5}M'_n(a,\omega)\,\mathrm{e}^{-k_nx}, \quad (67)$$
$$\bar{\varphi}_2=\sum_{n=1}^{5}M''_n(a,\omega)\,\mathrm{e}^{-k_nx}, \quad (68)$$
$$\bar{\varphi}^*=\sum_{n=1}^{5}M'''_n(a,\omega)\,\mathrm{e}^{-k_nx}, \quad (69)$$
$$\bar{T}=\sum_{n=1}^{5}M''''_n(a,\omega)\,\mathrm{e}^{-k_nx}, \quad (70)$$

where $M_n(a,\omega)$, $M'_n(a,\omega)$, $M''_n(a,\omega)$, $M'''_n(a,\omega)$ and $M''''_n(a,\omega)$ are some functions depending on a and ω, k_n^2 $(n=1,2,3,4,5)$ are the roots of the characteristic equation of Eq. (59).

Using Eqs. (66)–(70) in Eqs. (39) and (43), we obtain the following relations:

$$\bar{\psi}=\sum_{n=1}^{5}a_n^*M_n(a,\omega)\,\mathrm{e}^{-k_nx}, \quad (71)$$

$$\bar{\varphi}_2 = \sum_{n=1}^{5} b_n^* M_n(a,\omega)\,\mathrm{e}^{-k_n x}, \tag{72}$$

$$\bar{T} = \sum_{n=1}^{5} c_n^* M_n(a,\omega)\,\mathrm{e}^{-k_n x}, \tag{73}$$

$$\bar{\varphi}^* = \sum_{n=1}^{5} d_n^* M_n(a,\omega)\,\mathrm{e}^{-k_n x}, \tag{74}$$

where

$$a_n^* = \frac{A_2(k_n^2 - A_4)}{(k_n^4 - g_1 k_n^2 + g_2)}, \tag{75}$$

$$b_n^* = \frac{a_4 A_2(k_n^2 - a^2)}{(k_n^4 - g_1 k_n^2 + g_2)}, \tag{76}$$

$$c_n^* = \frac{a_6 A_7 k_n^4 - g_7 k_n^2 + g_8}{a_6 k_n^4 - g_3 k_n^2 + g_4}, \tag{77}$$

$$d_n^* = \frac{a_8 k_n^4 - g_5 k_n^2 + g_6}{a_6 k_n^4 - g_3 k_n^2 + g_4}. \tag{78}$$

4. Application

The plane boundary subjects to an instantaneous normal point force and the boundary surface is isothermal. The boundary conditions at the vertical plan $y = 0$ and in the beginning of the crack, at $x = 0$ are shown in Fig. 2.

(1) Mechanical boundary condition is that the surface of the half space obeys

$$\sigma_{zz} = -p(x), \quad |x| < a, \tag{79}$$

$$\sigma_{xz} = 0, \quad -\infty < x < \infty, \tag{80}$$

$$m_{xy} = 0, \quad -\infty < x < \infty, \tag{81}$$

$$\lambda_z = 0, \quad -\infty < x < \infty. \tag{82}$$

(2) Thermal boundary condition is that the surface of the half space subjects to a thermal shock,

$$T = f(x), \quad |x| < a; \qquad \frac{\partial T}{\partial z} = 0, \quad |x| > a. \tag{83}$$

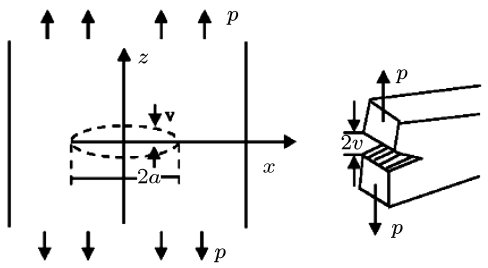


Fig. 2. Displacement of an external Mode-I crack.

Using Eqs. (31), (37), (39)–(43) with the dimensionless boundary conditions and using Eqs. (66)–(70), we obtain the expressions for the displacement components, the force stress, the coupled stress and the temperature distribution of the microstretch generalized thermoelastic medium as follows:

$$\bar{u} = \sum_{n=1}^{5} (\mathrm{i}aa_n^* - k_n) M_n(a,\omega) \mathrm{e}^{-k_n x}, \tag{84}$$

$$\bar{w} = \sum_{n=1}^{5} (\mathrm{i}a - a_n^* k_n) M_n(a,\omega)\,\mathrm{e}^{-k_n x}, \tag{85}$$

$$\bar{\sigma}_{zz} = \sum_{n=1}^{5} s_n M_n(a,\omega)\,\mathrm{e}^{-k_n x}, \tag{86}$$

$$\bar{\sigma}_{xz} = \sum_{n=1}^{5} r_n M_n(a,\omega)\,\mathrm{e}^{-k_n x}, \tag{87}$$

$$\bar{m}_{xy} = \sum_{n=1}^{5} q_n M_n(a,\omega)\,\mathrm{e}^{-k_n x}, \tag{88}$$

$$\bar{T} = \sum_{n=1}^{5} c_n^* M_n(a,\omega)\,\mathrm{e}^{-k_n x}, \tag{89}$$

$$\bar{\lambda} = \sum_{n=1}^{5} p_n M_n(a,\omega)\,\mathrm{e}^{-k_n x}, \tag{90}$$

where

$$\begin{aligned}
&s_n = f_1 d_n^* + \mathrm{i}\,a f_2(\mathrm{i}a - a_n^* k_n) - f_3 k_n(\mathrm{i}aa_n^* - k_n) - c_n^*,\\
&q_n = -f_7 b_n^* k_n, \quad p_n = f_8 d_n^*,\\
&r_n = \mathrm{i}\,a f_4(iaa_n^* - k_n) - k_n f_5(\mathrm{i}a - a_n^* k_n) + f_6 b_n^*,\\
&f_1 = \frac{\lambda_0}{\rho c_2^2}, \quad f_2 = \frac{\lambda + 2\mu + k}{\rho c_2^2}, \quad f_3 = \frac{\lambda}{\rho c_2^2},\\
&f_4 = \frac{\mu}{\rho c_2^2}, \quad f_5 = \frac{\mu + k}{\rho c_2^2}, \quad f_6 = \frac{k}{\rho c_2^2},\\
&f_7 = \frac{\gamma \omega^{*^2}}{\rho c_2^4}, \quad f_8 = \frac{\alpha_0 \omega^*}{\rho c_2^3}.
\end{aligned} \tag{91}$$

Applying the boundary conditions (79)–(83) at the surface $x = 0$ of the plate, we obtain a system of five equations. After applying the inverse of matrix method,

$$\begin{pmatrix} M_1 \\ M_2 \\ M_3 \\ M_4 \\ M_5 \end{pmatrix} = \begin{pmatrix} c_1^* & c_2^* & c_3^* & c_4^* & c_5^* \\ s_1 & s_2 & s_3 & s_4 & s_5 \\ r_1 & r_2 & r_3 & r_4 & r_5 \\ q_1 & q_2 & q_3 & q_4 & q_5 \\ p_1 & p_2 & p_3 & p_4 & p_5 \end{pmatrix}^{-1} \begin{pmatrix} f \\ -p \\ 0 \\ 0 \\ 0 \end{pmatrix}, \tag{92}$$

we obtain the values of the five constants M_n, $n = 1, 2, 3, 4, 5$. Hence, we obtain the expressions for the displacements, the force stress, the coupled stress and the temperature distribution of the microstretch generalized thermoelastic medium.

5. Numerical results and discussion

In order to illustrate our theoretical results obtained in the preceding section and to compare various theories of thermo-elasticity, we now present some numerical results. In the calculation, we take a magnesium crystal (Eringen, 1964) as the material subjected to mechanical and thermal disturbances. Since, ω is a complex constant, we take $\omega = \omega_0 + \mathrm{i}\zeta$ with $\omega_0 = -2$ and $\zeta = 1$. The physical constants used are:

$$\rho = 1.74 \times 10^3 \text{ kg} \cdot \text{m}^{-3}, \quad C_2 = 0.23 \times 10^2 \text{ m}^2 \cdot \text{s}^{-2},$$
$$\lambda = 9.4 \times 10^{11} \text{ kg} \cdot \text{m}^{-1} \cdot \text{s}^{-2}, \quad j = 0.2 \times 10^{-21} \text{ m}^3,$$
$$\mu = 4.0 \times 10^{11} \text{ kg} \cdot \text{m}^{-1} \cdot \text{s}^{-2}, \quad T_0 = 293 \text{ K}$$
$$k = 1.0 \times 10^{11} \text{ kg} \cdot \text{m}^{-1} \cdot \text{s}^{-2},$$
$$\gamma = 0.779 \times 10^{-8} \text{ kg} \cdot \text{m} \cdot \text{s}^{-2},$$
$$K = 0.6 \times 10^{-4} \text{ W} \cdot \text{m}^{-1} \cdot \text{K}^{-1},$$
$$\lambda_0 = 0.5 \times 10^{11} \text{ kg} \cdot \text{m}^{-1} \cdot \text{s}^{-2},$$
$$\lambda_1 = 0.5 \times 10^{11} \text{ kg} \cdot \text{m}^{-1} \cdot \text{s}^{-2},$$
$$\alpha_0 = 0.779 \times 10^{-4} \text{ kg} \cdot \text{m}^{-1} \cdot \text{s}^{-2}.$$

The variations of the components of displacements u and w, the temperature distribution T, the normal stress σ_{zz}, the tangential stress σ_{xz}, the tangential couple stress m_{xy} and the microstress λ_z versus distance x at the plane $z = -1$, $a = 1$, $f = 1$ and $p = -2$ based on the (CD) and the (L–S) theories have been shown by solid and dashed lines respectively for the generalized thermo-microstretch elastic (GTMSE) medium with ($\Omega = 0.2$) and without rotation ($\Omega = 0.0$). These distributions are shown graphically in Figs. 3–9 for thermal sources at $t = 0.1$. The distributions of displacements u and w, the temperature distribution T, the normal stress σ_{zz}, the tangential stress σ_{xz} and the tangential couple stress m_{xy} versus distance x at the plane $z = -1$, $t = 0.1$, $a = 1$, $f = 1$ and $p = -2$ based on the CD and the L–S theories have been shown graphically in Figs. 11–15 by solid and dashed lines respectively for the generalized micropolaer thermo-elasticity elastic (GMTE) medium without microstretch constants. Figures 16–23 compare the temperature T, the displacement component w , the force stresses components σ_{zz}, σ_{xz} , the tangential coupled stress m_{xy} and the microstress λ_z for three different values of z, namely $z = 1$, 0.9 and 0.8, under the GL theory. We notice that the results for the temperature, the displacement and the stress distribution with the relaxation time included in the heat equation are distinctly different from those without the relaxation time in the heat equation, because the thermal waves in the Fourier's theory travel at an infinite speed as opposed to the finite speed in the non-Fourier case. This demonstrates clearly the difference between the coupled and the generalized theories of thermo-elasticity.

5.1. Generalized thermo-microstretch elastic medium

For the GTMSE medium at $\Omega = 0.2$ and 0.0, results are shown graphically in Figs. 3–9. For the values of z, namely $z = 0.1$, were substituted in performing the computation. It should be noted (Fig. 3) that in this problem, the crack's size x is taken to be the length in this problem, so that $0 \le x \le 0.4$ for $\Omega = 0.0$ and $0 \le x \le 0.7$ for $\Omega = 0.2$, $z = 0$ represents the plane that the crack is symmetric with respect to. It is clear from the graph that T has a maximum value at the beginning of the crack ($0 \le x \le 1$ (for $\Omega = 0.2$)), and begins to fall just near the crack edge ($2.5 \le x \le 3.5$), where it experiences a sharp decrease (with a maximum negative gradient at the crack end). The value of temperature quantity converges to zero with the increasing distance x.

Figure 3 shows that in both theories (CD and L–S), the temperature for $\Omega = 0.0$ is smaller compared to that for $\Omega = 0.2$ in the ranges $0 \le x \le 1.1$ and $4 \le x \le 6.5$ and is larger in the range $1.1 \le x \le 4$, while it converges to zero for $x > 8$.

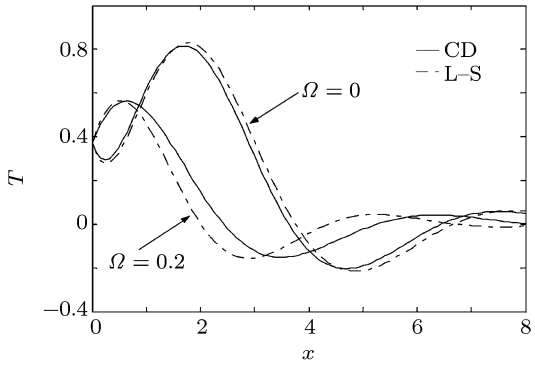


Fig. 3. Temperature distributions at different rotation speeds for GTMSE medium.

The behaviour of displacement component u in the CD and the L–S theories for the two different values of rotation is similar, as shown in Fig. 4. The values of displacement for $\Omega = 0.0$ are larger compared to those for $\Omega = 0.2$ in the ranges $0 \le x \le 1.5$ and $4.8 \le x \le 8$ and are smaller in the range $1.5 \le x \le 4.8$, while they converge to zero for $x \ge 8$.

The displacement component w in the CD and the L–S theories for the two different values of rotation is similar, as shown in Fig. 5. The values of displacement

for $\Omega = 0.2$ are larger compared to those for $\Omega = 0.0$ in the ranges $0 \leq x \leq 1.8$ and are smaller in the range $1.8 \leq x \leq 4.5$, while converge to zero for $x \geq 8$. From Fig. 4, we note that the horizontal displacement u begins with a decrease, then smooth increases again to reach its maximum magnitude just at the crack end and falls again to retain zero at infinity. In Fig. 5, we see that the displacement component w always starts with a zero (for $\Omega = 0.2$) value and terminates at the zero value, reaches a minimum value at the crack end and zero at the double of the crack size (state of particles equilibrium).

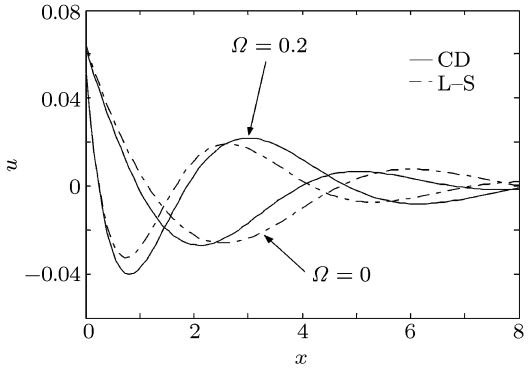


Fig. 4. Normal displacement distributions at different rotation speeds for GTMSE medium.

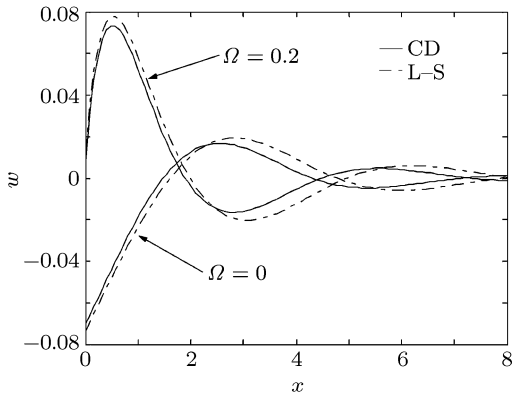


Fig. 5. Displacement distributions at different rotation speeds for GTMSE medium.

The displacements u and w show different behaviour, because the elasticity of the solid tends to resist vertical displacements in the case under investigation. Both components show different behaviour, the former tends to increase to a maximum just before the end of the crack, then falls to a minimum with a highly negative gradient, afterwards rises again to another maximum beyond the crack end.

Figure 6 shows that in both theories (CD and L–S), the values of normal stress σ_{zz} for $\Omega = 0.2$ are larger compared to those for $\Omega = 0.0$ in the range $0 \leq x \leq 3.8$, and are smaller in the range $3.8 \leq x \leq 6.3$, while converge to zero for $x \geq 8$. The stress component σ_{zz} reaches coincidence with negative value (Fig. 7) and satisfies the boundary condition at $x = 0$, reaches the maximum value near the end of crack and converges to zero with the increasing distance x.

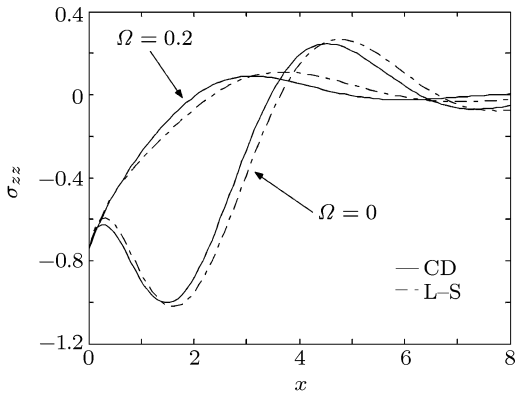


Fig. 6. Normal stress distributions at different rotation speeds for GTMSE medium.

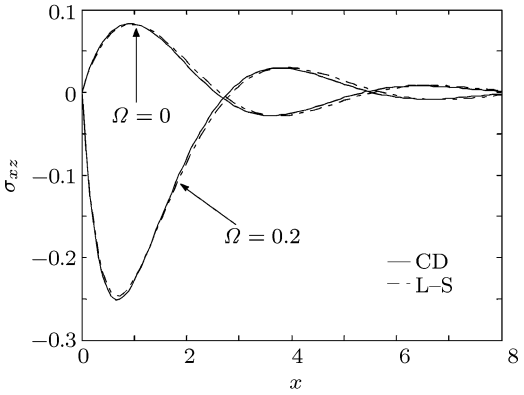


Fig. 7. Tangential stress distributions at different rotation speeds for GTMSE medium.

The behaviour of tangential stress component σ_{xz} in the theories CD and L–S is similar for both values of rotation. As depicted in Fig. 7, the values for $\Omega = 0.2$ are smaller in the ranges $0 \leq x \leq 2.5$ and $5.3 \leq x \leq 8$ compared to those for $\Omega = 0.0$ and are larger in the range $2.5 \leq x \leq 5.3$, while are the same for the three theories at $x \geq 8$. The stress component σ_{xz} satisfies the boundary condition at $x = 0$ and has a different behaviour. It decreases in the start and decreases (maximum (for $\Omega = 0.2$)) in the context of the three theories until reaching the crack end. These trends obey elastic and thermoelastic properties of the solid under investigation.

The behaviour of tangential coupled stress m_{xy} in both theories is opposite for both values of rotation constant, as depicted in Fig. 8. In the theories CD and L–S, the values of coupled stress for $\Omega = 0.2$ are larger in the ranges $0 \leq x \leq 2.7$ compared to those for $\Omega = 0.0$ and are the same for the two theories at

$x \geq 3$. The tangential coupled stress m_{xy} satisfies the boundary condition at $x = 0$. It increases in the start and decreases in the context of the two theories until reaching the crack end. Figure 9 shows that in the theories CD and L–S, the values of microstress component λ_z for $\Omega = 0.2$ are opposite and are smaller in the ranges $0 \leq x \leq 3$ and $6 \leq x \leq 8$ compared to those for $\Omega = 0.0$ and are larger in the range $3 \leq x \leq 6$, while are the same for the three theories at $x \geq 8$. The values of microstress for λ_z satisfy the boundary condition at $x = 0$, begin with an increase (for $\Omega = 0.0$) then decrease again to reach its minimum just near the crack end, reaching zero at the double of the crack size (state of particles equilibrium).

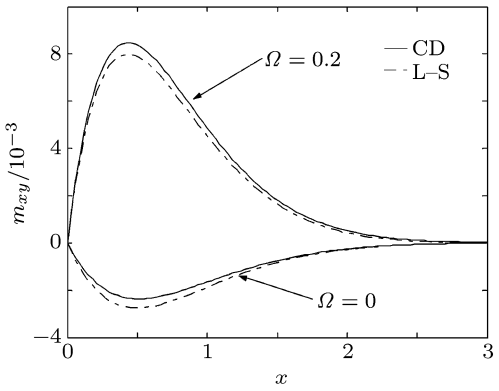


Fig. 8. Tangential couple stress distributions at different rotation speeds for GTMSE medium.

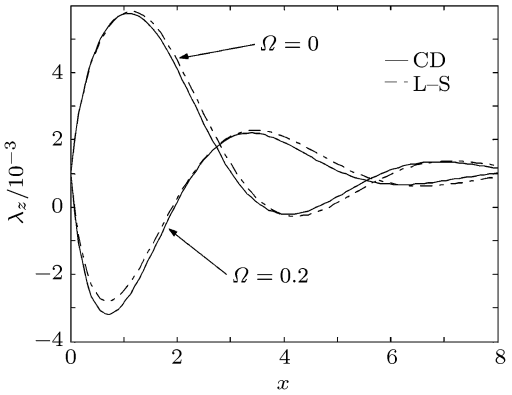


Fig. 9. Microstress distributions at different rotation speeds for GTMSE medium.

5.2. Generalized micropolaer thermoelasticity elastic medium

For the generalized micropolaer thermo-elasticity elastic (GMTE) medium in the presence ($\Omega = 0.2$) and in the absence ($\Omega = 0.0$) of rotation are shown graphically in Figs. 10–15. Figure 10 shows that for both theories the values of temperature in the GMTE medium are smaller for $\Omega = 0.2$ (the general behaviour) compared to those in the case of $\Omega = 0.0$.

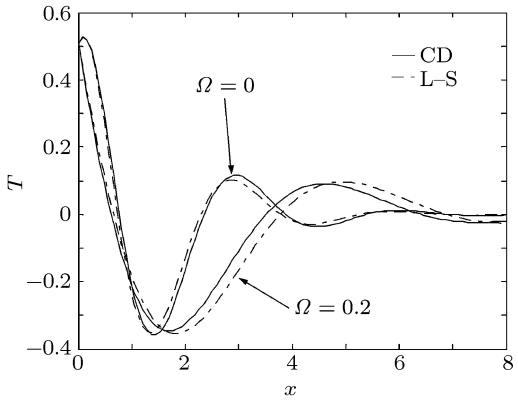


Fig. 10. Temperature distributions at different rotation speeds for GMTE medium.

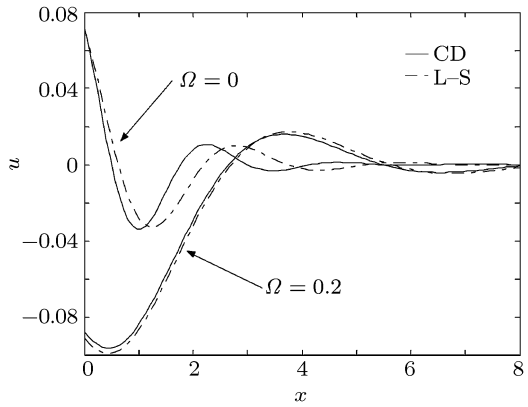


Fig. 11. Normal displacement distributions at different rotation speeds for GMTE medium.

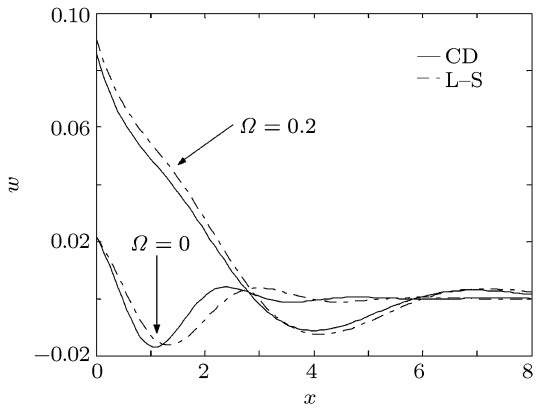


Fig. 12. Displacement distributions at different rotation speeds for GMTE medium.

The behaviour of displacement component u for the CD and the L–S theories is shown in Fig. 11. The values of normal displacement u in the GMTE medium are smaller for $\Omega = 0.2$ (the general behaviour) compared to those in the case of $\Omega = 0.0$.

As shown in Fig. 12, values of normal component of displacement w are smaller for $\Omega = 0.0$ compared to those in the case of $\Omega = 0.2$ (the general behaviour).

In Fig. 13, we compare the values of frequency of the normal stress. The values in the presence of rotation ($\Omega = 0.2$) are smaller compared to those in the absence ($\Omega = 0.0$) of rotation in the ranges $0 \leq x \leq 1.5$ and $3.8 \leq x \leq 6.5$, and are larger in the ranges $1.5 \leq x \leq 3.8$ and $x \geq 6.5$, while are the same for the theories at $x > 9$.

As shown in Fig. 14, values of tangential stress component σ_{xz} for $\Omega = 0.0$ are smaller compared to those for $\Omega = 0.2$ in the ranges $0 \leq x \leq 1.2$ and $3.8 \leq x \leq 7$ and larger in the range $1.2 \leq x \leq 3.8$, while are the same for the three theories at $x > 9.0$.

Figure 15 shows that in both theories, the values of coupled stress m_{xy} for $\Omega = 0.2$ are smaller compared to those for $\Omega = 0.0$ (the general behaviour).

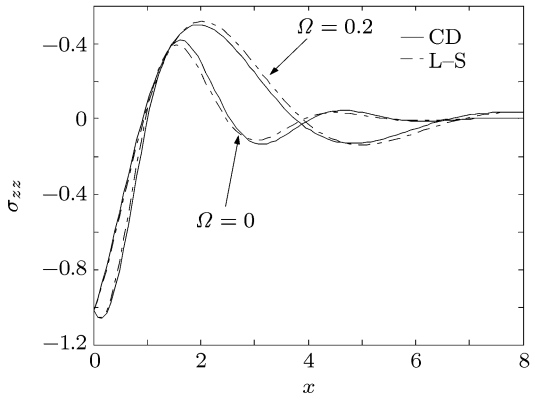


Fig. 13. Normal stress distributions at different rotation speeds for GMTE medium.

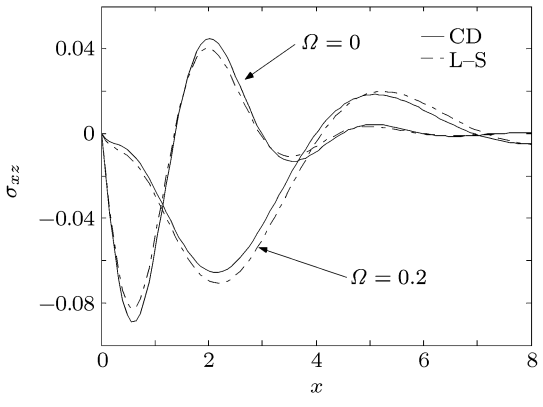


Fig. 14. Tangential stress distributions at different rotation speeds for GMTE medium.

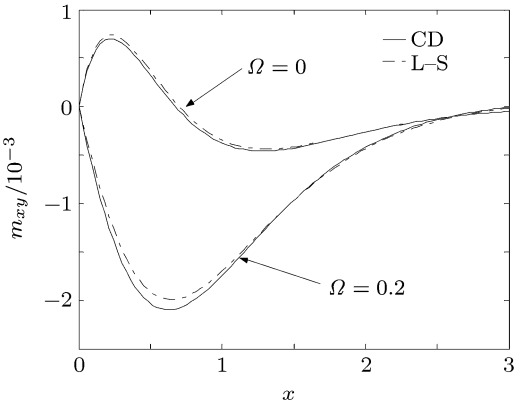


Fig. 15. Tangential couple stress distributions at different rotation speeds for GMTE medium.

5.3. Comparison

Figures 16–23 show a comparison of the temperature T, the displacement component w, the force stresses components σ_{zz}, σ_{xz}, the tangential coupled stress m_{xy} and the microstress λ_z, for three values of z, (namely $z = 1$, 0.9 and 0.8) under the GL theory. It is clear from the graph that T increases to a maximum value at the beginning of the crack and begin to fall just near the crack edge, where it experiences a sharp decrease (with maximum negative gradient at the crack end). Graph lines for different values of z show different slopes at the crack end accordingly. In other words, the temperature line for z=1 has the highest gradient compared with that of z=0.9 and 0.8 at the second range. In addition, all lines begin to coincide and to reach the reference temperature of the solid when the horizontal distance x is beyond the double of the crack size. These results agree with the physical reality for the behaviour of copper as a polycrystalline solid (It should be noted in Fig. 17).

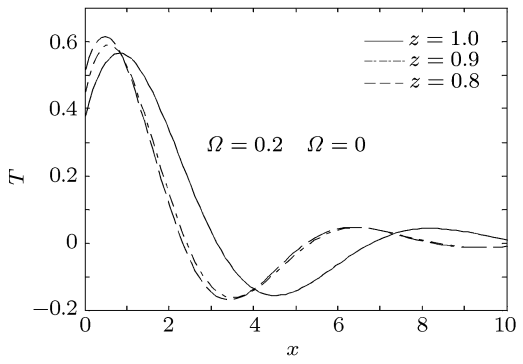


Fig. 16. Variations of temperature distribution T for different vertical distances under GL theory.

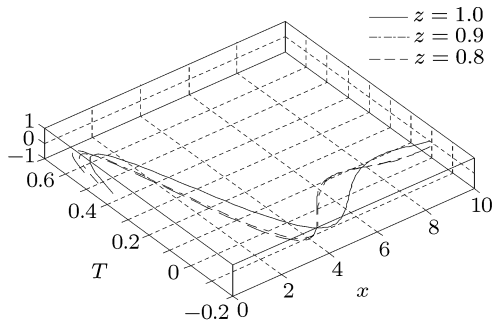


Fig. 17. Variations of temperature distribution T for different vertical distances under GL theory (3D).

As shown in Fig. 18, for the vertical displacement w, despite the peaks (for different vertical distances $z = 1$, 0.9 and 0.8) occur at equal value of x, the magnitude of the maximum displacement peak strongly depends on the vertical distance z. It is also clear that the rate of change of w increases with the decreasing z as we go further apart from the crack. On the other hand, Fig. 19 shows atonable increase of the vertical displacement w near the crack end. The vertical displacement w reaches minimum value beyond $x = 3$ and reaches zero at the double of the crack size (state of particles equilibrium).

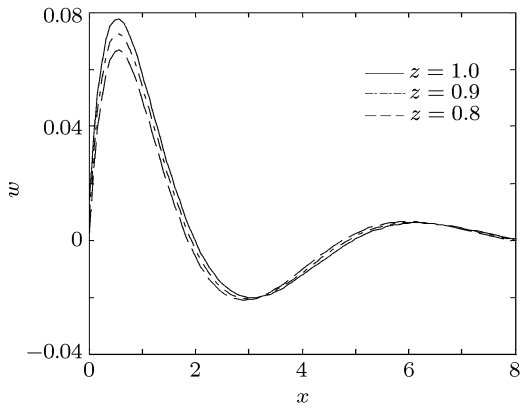


Fig. 18. Variations of displacement distribution w for different vertical distances, under GL theory.

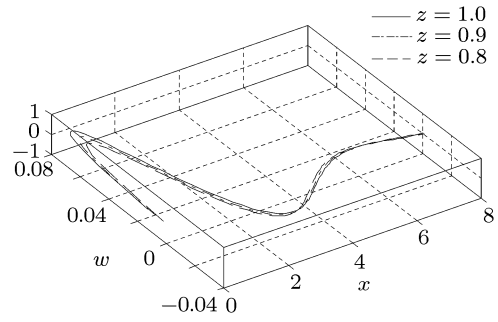


Fig. 19. Variations of displacement distribution w for different vertical distances under GL theory (3D).

As shown in Fig. 20, the vertical stresses σ_{zz} for different values of z show different slopes at the crack end. In other words, the σ_{zz} component for $z = 1$ has the highest gradient compared with that for $z = 0.9$ and 0.8 at the edge of the crack. In addition, all lines begin to coincide and to reach zero when the horizontal distance x is beyond the double of the crack size. Variation of z has a serious effect on both magnitudes of the mechanical stresses. These trends obey the elastic and the thermoelastic properties of the solid under investigation.

As shown in Fig. 21, the stress component σ_{xz} satisfies the boundary condition. The σ_{xz} for $z = 0.8$ has the highest gradient compared with that for z=0.9 and 1 (the general behaviour) and converge to zero when $x > 5$. These trends obey the elastic and the thermoelastic properties of the solid.

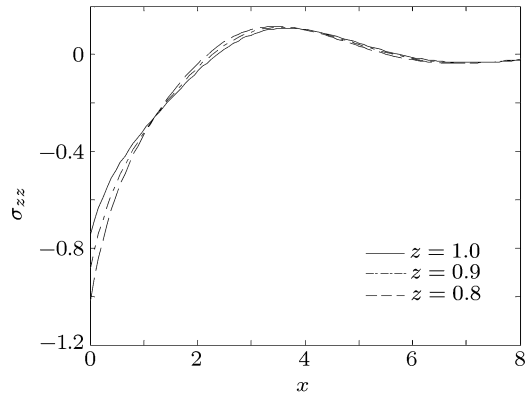


Fig. 20. Variations of stress distribution σ_{zz} for different vertical distances under GL theory.

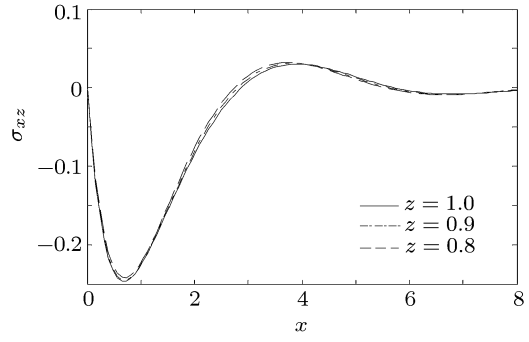


Fig. 21. Variations of stress distribution σ_{xz} for different vertical distances under GL theory.

As shown in Fig. 22, the tangential coupled stress m_{xy} increases in the start and decreases (minimum) in the context of the three values of z until reaching the crack end. For $z = 1$, the m_{xy} has the highest gradient compared with that for $z = 0.8$ and 0.9 at the edge of the crack. All lines begin to coincide when the

horizontal distance x is beyond the edge of the crack $x > 3$.

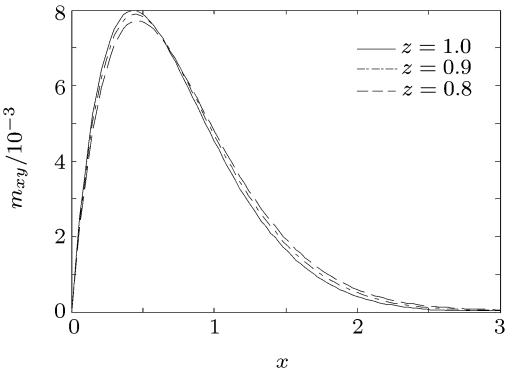


Fig. 22. Variations of tangential couple stress m_{xy} for different vertical distances under GL theory.

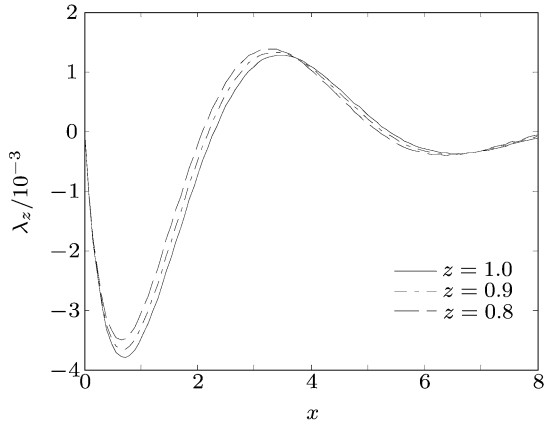


Fig. 23. Variations of microstress λ_z for different vertical distances under GL theory.

Figure 23 depicts the values of microstress for λ_z, which decreases in the start and start increases (maximum) in the context of the three values of z until nearly reaching the crack end. For $z = 0.8$, the microstress has the highest gradient compared with that for $z = 0.9$ and 1 at the edge of the crack. All lines begin to coincide and to reach zero when the horizontal distance x is beyond the double of the crack size.

6. Conclusion

A linear opening mode-I crack has been investigated and studied for the copper solid. Analytical solutions based upon normal mode analysis for the themoelastic problem in solids have been developed and utilized. Temperature, radial and axial distributions were estimated at different distances from the crack edge. The stresses distributions, the tangential coupled stress and the values of microstress were evaluated as functions of the distance from the crack edge. It is found that the cracks are stationary and external stress is demanded to propagate such cracks. The crack dimensions are significant to elucidate the mechanical structure of the solid. It can be concluded that a change of the volume is attended by a change of the temperature, while the effect of the deformation upon the temperature distribution is the subject of the theory of thermo-elasticity. The curves in the CD and the L–S theories decrease exponentially with the increasing x, which indicates that the thermoelastic waves are unattenuated and nondispersive, while purely thermoelastic waves undergo both attenuation and dispersion. In most figures, the physical quantities based on the L–S theory are lower compared with those based on the CD theory. The values of all the physical quantities converge to zero with an increase in the distance x and all functions are continuous. The presences of rotation and microstretch play significant roles in all physical quantities.

References

[1] Agarwal, V K 1979 *Acta Mech.* **31** 185
[2] Agarwal V K 1979 *Acta Mech.* **34** 181
[3] Schoenberg M and Censor D 1973 *Appl. Math.* **31** 115
[4] Puri P 1976 *Bull. DeL'Acad. Polon. Des. Sci. Ser. Tech.* **XXIV** 103
[5] Roy Choudhuri S K and Debnath L 1983 *Int. J. Eng. Sci.* **21** 155
[6] Roy Choudhuri S K and Debnath L 1983 *J. Appl. Mech.* **50** 283
[7] Othman M I A 2004 *Int. J. Solids Struct.* **41** 2939
[8] Othman M I A 2005 *Acta Mechanica.* **174** 129
[9] Othman M I A and Singh B 2007 *Int. J. Solids Struct.* **44** 2748
[10] Othman M I A and Song Y Q 2008 *Appl. Math. Modelling* **32** 811
[11] Eringen A C and Suhubi E S 1964 *Int. J. Engng. Sci.* **2** 1
[12] Eringen A C 1966 *J. Math. Mech.* **15** 909
[13] Othman M I A 2004 *Mechanics and Mechanical Engineering* **7** 165
[14] Eringen A C 1971 *Ari Kitabevi Matbassi, Istanbul* **24** 1
[15] Eringen A C 1968 *Theory of Micropolar Elasticity* (Vol. II) (New York: Academic Press) pp. 621–729
[16] Eringen A C 1990 *Int. J. Engng. Sci.* **28** 1291 1301
[17] Eringen A C 1999 *Microcontinuum Field Theories* I: *Foundation and Solids* (New York: Springer-Verlag)
[18] Iesau D and Nappa L 2001 *Int. J. Engng. Sci.* **39** 1815
[19] Iesau D and Pompei A 1995 *Int. J. Engng. Sci.* **33** 399
[20] de Cicco S 2003 *Int. J. Engng. Sci.* **41** 187
[21] Bofill F and Quintanilla R 1995 *Int. J. Engng. Sci.* **33** 2115
[22] de Cicco S and Nappa L 2000 *J. Math. Mech.* **41** 467
[23] de Cicco S and Nappa L 1999 *J. Thermal Stresses* **22** 565

[24] Green A E and Laws N 1972 *Arch. Ration. Mech. Anal.* **15** 47
[25] Lord H W and Şhulman Y 1967 *J. Mech. Phys. Solid* **15** 299
[26] Green A E and Lindsay K A 1972 *J. Elasticity* **2** 1
[27] Othman M I A and Lotfy Kh 2009 *MMMS* **5** 235
[28] Othman M I A, Lotfy Kh and Farouk R M 2009 *Acta Phys. Polonica* A **116** 185
[29] Othman M I A and Lotfy Kh 2010 *Int. Commun. Heat Mass* **37** 192
[30] Othman M I A, Lotfy Kh and Farouk R M 2009 *International Journal of Industrial Mathematics* **1** 87
[31] Othman M I A and Lotfy Kh 2010 *Engineering Analysis with Boundary Elements* **34** 229
[32] Dhaliwal R 1980 *External Crack due to Thermal Effects in an Infinite Elastic Solid with a Cylindrical Inclusion, Thermal Stresses in Server Environments* (New York: Plenum Press) pp. 665–692
[33] Hasanyan D, Librescu L, Qin Z and Young R 2005 *J. Thermal Stresses* **28** 729
[34] Ueda S 2003 *J. Thermal Stresses* **26** 311
[35] Elfalaky A and Abdel-Halim A A 2006 *J. Appl. Sci.* **6** 598